

An Inversion-based Measure of Memorization for Diffusion Models

Zhe Ma, Qingming Li, Xuhong Zhang, Tianyu Du,
Ruixiao Lin, Zonghui Wang, Shouling Ji, Wenzhi Chen
Zhejiang University

{mz.rs, liqm, zhangxuhong, zjradty, linruixiao, zhwang, sji, chenwz}@zju.edu.cn

Abstract

The past few years have witnessed substantial advances in image generation powered by diffusion models. However, it was shown that diffusion models are vulnerable to training data memorization, raising concerns regarding copyright infringement and privacy invasion. This study delves into a rigorous analysis of memorization in diffusion models. We introduce an inversion-based measure of memorization, *InvMM*, which searches for a sensitive latent noise distribution accounting for the replication of an image. For accurate estimation of the memorization score, we propose an adaptive algorithm that balances the normality and sensitivity of the inverted distribution. Comprehensive experiments, conducted on both unconditional and text-guided diffusion models, demonstrate that *InvMM* is capable of detecting heavily memorized images and elucidating the effect of various factors on memorization. Additionally, we discuss how memorization differs from membership. In practice, *InvMM* serves as a useful tool for model developers to reliably assess the risk of memorization, thereby contributing to the enhancement of trustworthiness and privacy-preserving capabilities of diffusion models.

1. Introduction

Diffusion Models (DMs) [22, 49] have shown impressive capability in the generation of images [40, 41], videos [6], 3D point cloud [34], etc. These techniques lay the foundation for commercial systems or communities such as Stable Diffusion [41], Midjourney [1], DALL-E [3, 40] and Imagen [42], which have attracted millions of active users. The popularity of diffusion models can be attributed to the hierarchical denoising procedure, which offers high stability for training on billions of data [45] and scalability for multimodal conditional generation [40, 42].

However, large-scale data sets used to train the prevalent DMs, e.g., the open-source image-caption dataset LAION [45], are widely acknowledged to contain content that will raise concerns regarding copyright infringe-

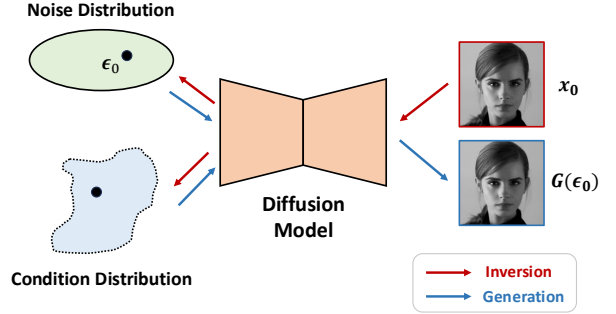


Figure 1. Schematic illustration of diffusion model inversion, optionally with conditions.

ment, privacy invasion, etc. For example, recent reports revealed that LAION could refer to photographers’ work without authorization [18] and contain private medical photographs [2]. With the uncured data for training, diffusion models are likely to generate content that infringes the creators’ rights or exposes private information [9, 46]. In this work, we focus on memorization in DMs, one of the most critical issues of training data misuse.

Memorization usually manifests itself at sampling time, when a model generates images closely resembling training images. It can turn into a problem both technically and practically. Technically, memorization indicates failure of generalization to some degree because a probabilistic generative model is supposed to produce novel and diversified images rather than simply replicate those in the training set. Practically, memorization might also raise ethical and legal concerns. First, even the model developers are authorized to train their model with protected images, the image owners will never expect their works to be exposed to arbitrary users due to memorization as this would cause indiscriminable dissemination, violating the contextual integrity [36]. Second, in past years, text-to-image models have been facing lawsuits for generating derivative images that mimic the style of artists. Compared to derivative generations whose legality is still in pending [44], exact replication of copy-

righted images is undisputedly intolerable. Finally, a series of works [24, 37] have proposed to use synthetic data in place of real data to prevent sharing of private information. For this goal, potential memorization should also be carefully circumvented.

Recent studies [9, 50, 51, 57] confirm the existence of memorization in DMs in a two-stage way. They first randomly draw samples from the model and then detect risky generations of low diversity [9], search for nearest neighbors in the training set [50, 51] or identify abnormal prediction errors [57]. However, conducting a practical analysis of memorization with these approaches still faces challenges. Transforming the memorization of an image to the presence or absence in samples from the model is not a reliable and efficient solution. While certain images do not appear in a set of samples, it does not demonstrate that they are not highly memorized [54]. For DMs with large latent space, adequate samples should be tested to ensure as complete coverage of the latent space as possible, which usually requires up to millions of testings [9, 57]. Furthermore, things will get much more complicated in conditional DMs, e.g., text-to-image generation. The additional conditions expand the input space of DMs, making the memorization of an image depend on the specific condition. Recent studies use training captions to induce the model to emit corresponding highly memorized training images. However, it still remains unknown that whether the other images not triggered by their coupled captions are also to high extent of memorization.

To address these challenges, we propose an Inversion-based Measure of Memorization (InvMM¹) for DMs, a continuous instance-level measure that takes an image as input, outputs a scalar quantifying its level of memorization. As shown in Fig. 1, the inversion process locates a sensitive latent noise distribution and optionally another condition distribution for the target image, such that generating with noise and condition drawn from the inverted distributions will produce samples exactly the same as the target image. InvMM is then defined as the minimum KL divergence to the standard Gaussian distribution and estimated through an adaptive optimization algorithm. Compared to existing studies, InvMM is more reliable and efficient by explicitly searching for all potential sensitive inputs and avoiding to collect any conditions (e.g., prompts). It enables us to discover highly memorized images, claim the safety against memorization for normal images, determine the best training setting, etc. In summary, we make the following contributions in this paper:

- We propose a novel measure of memorization for DMs, that is more reliable and efficient.
- For accurate estimation of the measure, we provide an

adaptive algorithm that alleviates overestimation and underestimation.

- We validate the effectiveness of our measure through comprehensive experiments across four datasets, encompassing both unconditional and text-guided DMs.

2. Related work

2.1. Memorization of generative models

Memorization has raised wide attention on various generative models, including GAN [17], VAE [29], language models [7] and DM [49]. There have been studies on training algorithms [4, 22, 43] and evaluation protocols [19] to improve the generalization ability of generative models that would potentially circumvent memorization. Empirical and theoretical studies also find that dataset complexity and size [15, 50], training time [53], training data duplication [10, 59] and model capacity [5, 10] are influential factors of memorization. Several works [53, 58] focus on the latent space (noise space) to analyze memorization. Nagarajan et al. [53] demonstrate that when trained on sufficient random noise vectors, a generator is guaranteed to memorize training data. Webster et al. [58] measure overfitting of GANs via the reconstruction error at the optimal noise vector. We take a similar perspective on the latent space to analyze memorization while aim to reach an instance-level measure of memorization rather than reveal overall properties of models. In addition, Van der Burg et al. [54] also propose an instance-level measure of memorization as the changed likelihood of one sample when removing it from the training set. However, as discussed by them, the measure is not necessarily comparable between datasets, which is important to understand the true level of memorization.

Specifically for diffusion models, recent research [9, 50, 51] demonstrates that memorization occurs in text-to-image diffusion models. Some heavily memorized images are discovered from numerous generated samples by membership inference [9] or searching for the most similar training images with image matching models [50]. Subsequently, Webster [57] provides more efficient attacks to extract training images from text-to-image models. Wen et al. [61] focus on the detection of abnormal prompts that will trigger generation of training images. In response to the disclosed threats, Vyas et al. [55] propose a provable copyright protection method to prevent replication of sensitive training images. The model is trained to align with a safe model that does not take sensitive data for training. Chen et al. [12] prevent training data replication by a modified sampling procedure that dynamically twists the sampling direction far away from any training points. Our method complements existing studies as a effective way to quantify memorization for any sample (not necessarily training samples).

¹The source code can be found at <https://github.com/Maryeon/InvMM>.

2.2. Inversion of diffusion models

Inversion techniques in diffusion models are widely studied for image editing [16, 35, 63], copyright protection [62], generated content detection [11, 56], etc. Through inversion, the object, style and concept contained in the source images can be compressed in latent noises or input token embeddings (for text-to-image generation). Then the inverted latent noises or input token embeddings are utilized to generate same/similar images that preserve the desired content.

We leverage inversion techniques to analyze memorization in diffusion models. In contrast, we invert a sample to a distribution consisting of all feasible latent vectors rather than to a single vector [11, 16, 35, 56, 62]. We also adopt more efficient training objective for inversion, without the need to iteratively invert a specific sampling procedure [11, 35, 56, 62].

3. Background

Basically, DMs [22, 49] are likelihood-based generative models that learn to maximize the likelihood $p_\theta(\mathbf{x}_0)$ of observed data \mathbf{x}_0 . Directly calculating $p_\theta(\mathbf{x}_0)$ is intractable for continuous data such as image. By contrasting to a sequence of latent variables $\mathbf{x}_{1:T}$, the log-likelihood $\log p_\theta(\mathbf{x}_0)$ can be maximized indirectly by maximizing its variational lower bound [28, 33]:

$$\log p_\theta(\mathbf{x}_0) = \log \int p_\theta(\mathbf{x}_{0:T}) d\mathbf{x}_{1:T} \quad (1)$$

$$\geq \mathbb{E}_{q(\mathbf{x}_{1:T}|\mathbf{x}_0)} \left[\log \frac{p_\theta(\mathbf{x}_{0:T})}{q(\mathbf{x}_{1:T}|\mathbf{x}_0)} \right] \quad (2)$$

Assume both transitions $p_\theta(\mathbf{x}_{0:T})$ and $q(\mathbf{x}_{1:T}|\mathbf{x}_0)$ are Markov chains, i.e., $q(\mathbf{x}_{1:T}|\mathbf{x}_0) = \prod_{t=1}^T q(\mathbf{x}_t|\mathbf{x}_{t-1})$, $p_\theta(\mathbf{x}_{0:T}) = p(\mathbf{x}_T) \prod_{t=1}^T p_\theta(\mathbf{x}_{t-1}|\mathbf{x}_t)$, the variational lower bound in Eq. (2) expands as:

$$\begin{aligned} \log p_\theta(\mathbf{x}_0) &\geq \mathbb{E}_{q(\mathbf{x}_1|\mathbf{x}_0)} [\log p_\theta(\mathbf{x}_0|\mathbf{x}_1)] \\ &\quad - \sum_{t=2}^T \mathbb{E}_{q(\mathbf{x}_t|\mathbf{x}_0)} [D_{\text{KL}}(q(\mathbf{x}_{t-1}|\mathbf{x}_t, \mathbf{x}_0) \parallel p_\theta(\mathbf{x}_{t-1}|\mathbf{x}_t))] \end{aligned} \quad (3)$$

$$- D_{\text{KL}}(q(\mathbf{x}_T|\mathbf{x}_0) \parallel p(\mathbf{x}_T)) \quad (4)$$

where $p(\mathbf{x}_T)$ is generally assumed to be a simple distribution such as standard Gaussian $\mathcal{N}(\mathbf{0}, \mathbf{I})$.

The transition $q(\mathbf{x}_{1:T}|\mathbf{x}_0)$ is not learned but replaced by a manually crafted non-parametric diffusion process. The transition $p_\theta(\mathbf{x}_{0:T})$ is the corresponding reverse (or generation, sampling) process. The diffusion process gradually adds Gaussian noises to the input \mathbf{x}_0 according to a weight

schedule $\alpha_{1:T}$:

$$\mathbf{x}_t = \sqrt{\alpha_t} \mathbf{x}_{t-1} + \sqrt{1 - \alpha_t} \boldsymbol{\epsilon}_{t-1}, \boldsymbol{\epsilon}_{t-1} \sim \mathcal{N}(\mathbf{0}, \mathbf{I}) \quad (5)$$

$$\mathbf{x}_t = \sqrt{\bar{\alpha}_t} \mathbf{x}_0 + \sqrt{1 - \bar{\alpha}_t} \boldsymbol{\epsilon}_0, \boldsymbol{\epsilon}_0 \sim \mathcal{N}(\mathbf{0}, \mathbf{I}) \quad (6)$$

where $\bar{\alpha}_t = \prod_{i=1}^t \alpha_i$ decreases over time and finally to almost zero at the last step T , such that $q(\mathbf{x}_T|\mathbf{x}_0)$ approaches to a standard Gaussian and thus Eq. (4) approximately equals to 0.

If the diffusion process is divided into sufficient steps, each reverse transition $p_\theta(\mathbf{x}_{t-1}|\mathbf{x}_t)$ can also be approximated by a Gaussian transformation with learnable parameters that is trained to match the corresponding posterior diffusion transition $q(\mathbf{x}_{t-1}|\mathbf{x}_t, \mathbf{x}_0)$. Omitting further details [33], the following simplified objective [22] as an estimate of the variational lower bound is commonly used for training:

$$l_{de} = \mathbb{E}_{\boldsymbol{\epsilon}_0 \sim \mathcal{N}(\mathbf{0}, \mathbf{I}), t \sim \mathcal{U}\{1, T\}} [\|\boldsymbol{\epsilon}_0 - \boldsymbol{\epsilon}_\theta(\mathbf{x}_t, t)\|_2^2] \quad (7)$$

where $\boldsymbol{\epsilon}_\theta$ is a neural network that takes the noisy data \mathbf{x}_t and timestep t as input and predicts the added noise $\boldsymbol{\epsilon}_0$. After training, the vanilla sampling procedure starts with a random Gaussian noise $\mathbf{x}_T \sim \mathcal{N}(\mathbf{0}, \mathbf{I})$ and removes the predicted noise stepwise. However, it is extremely slow to generate an image as it must invoke the network $\boldsymbol{\epsilon}_\theta$ for T times (typically 1000 steps). To mitigate the problem, a variety of efficient sampling algorithms are proposed, such as DDIM sampler [52] and PLMS sampler [32].

4. Inversion-based measure

Given an image \mathbf{x}_0 , we aim to measure to what extent \mathbf{x}_0 is memorized by a diffusion model (DM). We propose to invert the image into a latent noise distribution, such as noise vectors drawn from it will lead to replication of the image \mathbf{x}_0 . Our memorization measure is established in this inversion process. In this section, we introduce a sensitivity definition of the inverted noise distribution (Sec. 4.1), elaborate the memorization measure (Sec. 4.2) and give an adaptive algorithm for its calculation (Sec. 4.3). Ultimately, we present an example to measure memorization in conditional DM, specifically text-to-image DM (Sec. 4.4).

4.1. Sensitivity of latent distribution

The diversity of DM generated content lies in the randomness of latent noise vectors. Starting from different noise vectors, the generated content generally vary. In the context of memorization, this motivates us to search for *sensitive noise vectors* that will replicate the target image. We then figure out “how many” sensitive noise vectors there are and adopt it as a meaningful measure.

Considering the fact that the common latent noise is sampled from a standard Gaussian distribution, we correspond-

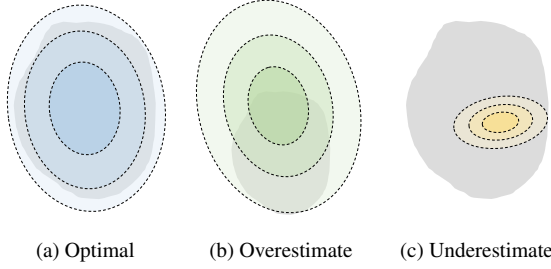


Figure 2. Illustration of our memorization measure. The gray blocks indicate the distribution of sensitive latent noise vectors.

ingly assume the sensitive noise vectors follow a distribution $q_\varphi(\epsilon_0|x_0)$ with learnable parameters φ . The sensitivity function $\mathcal{S}(q_\varphi)$ of a noise distribution can be defined as the probability that generated image $G(\epsilon_0)$ obtained from random noise $\epsilon_0 \sim q_\varphi(\epsilon_0|x_0)$ replicates the target image x_0 :

$$\mathcal{S}(q_\varphi) = \int \mathbf{1}_{d(G(\epsilon_0), x_0) \leq \beta} q_\varphi(\epsilon_0|x_0) d\epsilon_0 \quad (8)$$

where $\mathbf{1}_v$ is an indicator function that equals 1 if v is true and 0 otherwise, $d(\cdot, \cdot)$ is a distance metric between two images and β is an appropriate threshold.

The choice of the distance metric depends on specific applications. In applications that accept derivative generation, a strict metric that only detects eidetic generation can be utilized. While under some circumstances even similar generation should be circumvented, a looser metric is needed. In this work, we consider exact replication that the generated image and target image are exactly the same, following previous work [9]. This consideration to some extent reduces the ambiguity of determining the similarity of two images. Following the investigation of Somepalli et al. [50], we implement the metric as the Euclidean distance between embeddings extracted by the pre-trained copy detection model SSCD [38].

4.2. Quantify memorization

Based on the definition of sensitivity, we propose an **Inversion-based Measure of Memorization (InvMM)**, as the best achievable normality of $q_\varphi(\epsilon|x)$ under the condition that $\mathcal{S}(q_\varphi) = 1$:

$$\begin{aligned} \min_{\varphi} D_{\text{KL}}(q_\varphi(\epsilon_0|x) \parallel p(\epsilon_0)) \\ \text{s.t. } \mathcal{S}(q_\varphi) = 1 \end{aligned} \quad (9)$$

where $p(\epsilon_0)$ is the prior distribution used in DM, which is often selected to be standard Gaussian. The normality of inverted noise distribution is the KL divergence to the prior.

Explaining InvMM. Partitioning the normality gives us

a more intuitional understanding of the measure. Notice that

$$\begin{aligned} D_{\text{KL}}(q_\varphi(\epsilon_0|x_0) \parallel p(\epsilon_0)) = \\ H(q_\varphi(\epsilon_0|x_0), p(\epsilon_0)) - H(q_\varphi(\epsilon_0|x_0)) \end{aligned} \quad (10)$$

where $H(q_\varphi(\epsilon_0|x_0), p(\epsilon_0))$ is the cross entropy between the inverted distribution and the prior distribution, $H(q_\varphi(\epsilon_0|x_0))$ is the differential entropy of the inverted distribution. Minimizing the normality thus encourages a distribution as close to the prior distribution as possible, meanwhile with the largest entropy. For the cross entropy, following the Jensen’s inequality, $-H(q_\varphi(\epsilon_0|x_0), p(\epsilon_0)) = \mathbb{E}_{q_\varphi(\epsilon_0|x_0)}[\log p(\epsilon_0)] \leq \log \int q_\varphi(\epsilon_0|x_0)p(\epsilon_0)d\epsilon_0$. The term $q_\varphi(\epsilon_0|x_0)p(\epsilon_0)$ is proportional to the probability of a random noise ϵ_0 , with probability density $q_\varphi(\epsilon_0|x_0)$, to be sampled from the prior distribution with probability density $p(\epsilon_0)$. In the sense, minimizing the cross-entropy improves the probability that sensitive noise vectors regarding an image x_0 are sampled in the normal usage of DM, thus reflects the worst-case memorization of the image. For the differential entropy, maximizing it will produce a noise distribution involving “as much” sensitive noise vectors as possible. In the extreme case, suppose a uniform distribution over the entire latent space having the largest entropy, it means that any noise in the space can cause replication of the target training sample.

InvMM requires to achieve the best trade-off between improving normality and meeting the sensitivity condition. Different images to varied extent of memorization may reach different trade-off. Figure 2 illustrates the optimal solution compared to suboptimal choices. Overestimate of memorization produces a distribution with good normality but low sensitivity (Fig. 2b). Conservative inversion of the latent distribution perfectly meets the sensitivity condition but underestimates memorization (Fig. 2c).

4.3. Adaptive algorithm

We then describe how to solve the inversion problem and introduce an adaptive algorithm to calculate the proposed measure.

Transforming the inversion problem. It is intractable to directly calculate the sensitivity function. For diffusion models, it can be achieved by minimizing the denoising error l_{de} (see Eq. (7)) as a proxy. As can be expected, when l_{de} decreases to a certain level, $\mathcal{S}(q_\varphi)$ will approach 1.

Moreover, denote the KL divergence in Eq. (9) by l_{kl} , the optimization problem can be solved by Lagrangian method:

$$\min_{\varphi, \lambda} l_{de}(x_0; \varphi) + \lambda l_{kl}(x_0; \varphi), \lambda > 0 \quad (11)$$

where $\lambda > 0$ is a multiplier. Note that we attach the multiplier to l_{kl} to ensure adequate optimization of the denoising error l_{de} .

Different from the standard ϵ_0 -prediction denoising error, we adopt \mathbf{x}_0 -prediction denoising error, which shows more stable inversion efficacy in practice:

$$\begin{aligned} l_{de} &= \mathbb{E}_{q_{\varphi}(\epsilon_0|\mathbf{x}_0), t} [\|\mathbf{x}_0 - \mathbf{x}_{\theta}(\mathbf{x}_t, t)\|_2^2] \\ &= \frac{1 - \bar{\alpha}_t}{\bar{\alpha}_t} \mathbb{E}_{q_{\varphi}(\epsilon_0|\mathbf{x}_0), t} [\|\epsilon_0 - \epsilon_{\theta}(\mathbf{x}_t, t)\|_2^2] \end{aligned} \quad (12)$$

where \mathbf{x}_t is obtained as in Eq. (6) with added noise drawn from q_{φ} rather than standard Gaussian.

For the noise distribution $q_{\varphi}(\epsilon_0|\mathbf{x}_0)$, we assume it to be a multivariate Gaussian $\mathcal{N}(\boldsymbol{\mu}, \boldsymbol{\sigma}^2)$ with learnable mean $\boldsymbol{\mu}$ and diagonal variance $\boldsymbol{\sigma}^2$, i.e., $\varphi = (\boldsymbol{\mu}, \boldsymbol{\sigma}^2)$. Then InvMM has a closed-form expression $\frac{1}{2} \sum_i (\boldsymbol{\mu}_i^2 + \boldsymbol{\sigma}_i^2 - \log \boldsymbol{\sigma}_i^2 - 1)$. Although the true distribution of sensitive latent noise might not be fully captured by a Gaussian distribution, we choose this modeling for simplicity and find it effective in experiments.

Algorithm 1 InvMM: adaptive weight tuning algorithm.

Input: Noise prediction network ϵ_{θ} , target image \mathbf{x}_0 , optimization iteration S , observation cycle C , weight increment δ , threshold ξ , learning rate γ

- 1: Initialize $\varphi \leftarrow (\boldsymbol{\mu} \leftarrow \mathbf{0}, \boldsymbol{\sigma} \leftarrow \mathbf{I}), \lambda \leftarrow 1, l_{de}^p \leftarrow +\infty, \text{success} \leftarrow \text{FALSE}$
- 2: **for** $i \leftarrow 1$ to S **do**
- 3: $\mathcal{L} \leftarrow l_{de}(\mathbf{x}_0; \varphi) + \lambda l_{kl}(\mathbf{x}_0; \varphi)$
- 4: $\varphi \leftarrow \varphi - \gamma \nabla_{\varphi} \mathcal{L}$
- 5: **if** $i > 1$ **and** $i \% C = 0$ **then**
- 6: **if** $l_{de} - l_{de}^q < \xi$ **then**
- 7: $\lambda \leftarrow \lambda / 2$
- 8: **else**
- 9: $\lambda \leftarrow \lambda + \delta$
- 10: $l_{de}^q \leftarrow l_{de}$
- 11: **if** $\mathcal{S}(q_{\varphi}) = 1$ **then**
- 12: $\text{success} \leftarrow \text{TRUE}$
- 13: **break**
- 14: **else**
- 15: $\lambda \leftarrow \lambda + \delta$
- 16: **if** success **then**
- 17: **return** $\frac{1}{2} \sum_i (\boldsymbol{\mu}_i^2 + \boldsymbol{\sigma}_i^2 - \log \boldsymbol{\sigma}_i^2 - 1)$
- 18: **else**
- 19: **return** $+\infty$

Adaptive weight tuning. To achieve the best trade-off, the weight λ should be adjusted appropriately for different samples. However, it cannot be optimized via gradient descent together with φ . As the gradient w.r.t. λ is l_{kl} , which is always nonnegative, λ will gradually decrease to 0 and l_{kl} will be totally ignored. To solve the problem, we propose an adaptive weight tuning algorithm that allows dynamic change of λ during optimization, based on an additive increase/multiplicative decrease scheme similar to congestion control of TCP protocol, as in Algorithm 1, line 6-9.

Specifically, we monitor the denoising error l_{de} every C steps during the optimization process and divide the weight λ by half if no significant improvement of denoising error is observed in the cycle. Otherwise, λ slowly increases by a small increment δ each step. In this way, λ is adaptively adjusted for different samples to balance the normality and denoising error. When the normality is too strong to further reduce the denoising error, thus to meet the sensitivity condition, it is immediately down-weighted. Otherwise, we gradually strengthen it for better normality. We also perform early stop (line 11-13) when the sensitivity condition is reached to avoid unnecessary normality degradation (underestimate). The sensitivity condition is tested via the Monte Carlo method. Random latent vectors are drawn and used to generate samples. If the distance between any of them and the target image is lower than the threshold β , then the inversion is successful. There are cases that only partial samples replicate that target image in the end. We still consider such cases as insignificant memorization and flag them as unsuccessful.

4.4. Text-to-image DM

For text-to-image DM, we model the prompt part as a distribution as well and optimize it simultaneously with the noise distribution. Suppose each input prompt is tokenized into maximum N tokens $\boldsymbol{\omega} = [\boldsymbol{\omega}_1, \boldsymbol{\omega}_2, \dots, \boldsymbol{\omega}_N]$. Motivated by Guo et al. [20], we learn a $|\mathcal{V}|$ -dimensional categorical distribution over the vocabulary \mathcal{V} for each token $\boldsymbol{\omega}_i$. Let token $\boldsymbol{\omega}_i$ follows a categorical distribution with probabilities $\boldsymbol{\pi}_{i,j}$, where $\sum_{j=1}^{|\mathcal{V}|} \boldsymbol{\pi}_{i,j} = 1$. $\boldsymbol{\pi}_{i,j}$ can be parameterized and optimized.

Because sampling from categorical distribution is non-differentiable, we adopt the Gumbel-Softmax reparameterization [23] to obtain smoothed sample $\tilde{\boldsymbol{\omega}}_i$. Given the smoothed token $\tilde{\boldsymbol{\omega}}_i$, it can be converted to token embedding as a linear combination of vocabulary embeddings $e(\tilde{\boldsymbol{\omega}}_i) = \sum_{j=1}^{|\mathcal{V}|} \tilde{\boldsymbol{\omega}}_{i,j} e(j)$, where $e(j)$ is the pretrained token embedding of the j -th token. A proper choice of the prompt distribution is critical for inversion on text-to-image DM. We provide a comprehensive analysis in the supplementary material.

5. Experiment

In this section, we conduct a series of experiments from different perspectives to demonstrate the validity of InvMM. First, we conduct controlled studies to verify the effectiveness of the adaptive algorithm (Sec. 5.2). Based on this, we show that InvMM can accurately detect highly memorized images (Sec. 5.3) and elucidate the influence of various factors on memorization (Sec. 5.4). Finally, we discuss how memorization differs from membership (Sec. 5.5).

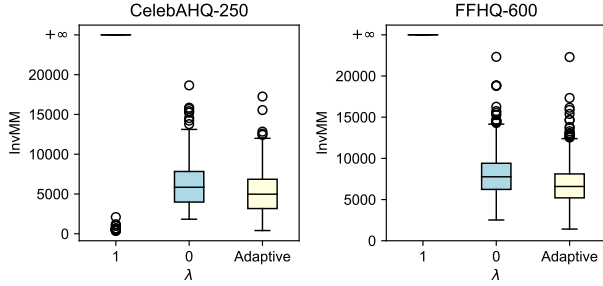


Figure 3. The influence of weight λ on measuring memorization.

5.1. Experiment setup

Dataset. We use four datasets for evaluation, i.e., CIFAR-10 [30], CelebAHQ [25], FFHQ [26] and LAION-Aesthetics V2 [45]. For subsequent experiments, we construct four randomly sampled subsets of CelebAHQ and FFHQ, CelebAHQ-250, CelebAHQ-2.5k, FFHQ-600 and FFHQ-6k. We ensure that the larger subset includes the smaller subset. The LAION dataset is extremely large. To keep computational costs manageable, we collect a subset of images. We first include 76 heavily memorized images discovered by Webster [57]. We call this set of images the *confirmed* set. Furthermore, we collected another 50 images with high duplication rates according to the statistics from Webster et al [59]. This set of suspects, named as the *suspicious* set, are assured to be disjoint with the *confirmed* set. Images in the *confirmed* set can be triggered by their training captions while those in the *suspicious* set cannot. Finally, another 50 randomly sampled images are used for comparison, referred to as the *normal* set.

Diffusion Models. Following the implementations of DDPM [22] and Latent Diffusion Model (LDM) [41], we train DDPM on CIFAR-10 and LDM on the subsets of CelebAHQ and FFHQ. Pre-trained LDMs on the whole CelebAHQ and FFHQ are also used. For text-to-image generation, we utilize Stable Diffusion (SD) v1.4 and v2.1 trained on LAION.

Inversion. The experiment setting and additional results, including prompt inversion for SD, are deferred to the supplementary material.

5.2. Adaptive algorithm

The core design of Algorithm 1 is the dynamic reweighting of the two loss items. To verify its effectiveness, we compare to fixed weights $\lambda = 1$ and $\lambda = 0$. $\lambda = 1$ equals DM’s original training objective (Eqs. (3) and (4)) and $\lambda = 0$ totally ignores the normality constraint.

A comparison of the resulting memorization score under different settings can be observed in Fig. 3. Fixing λ to 1 cannot successfully invert most images: 92.4% and 99.7%



Figure 4. Random samples generated using latent noise vectors drawn from inverted distributions. The original training images are in the first column within each block.

Metric	DDPM (CIFAR-10)		SD v1.4 (LAION)	
	AUC	TPR@1%FPR	AUC	TPR@1%FPR
ϵ_0 -loss	0.981	0.414	1.000	1.000
x_0 -loss	0.180	0.000	0.992	0.961
M^{LOO} [54]	0.418	0.000	-	-
Wen [61]	-	-	1.000	1.000
InvMM*	-	-	1.000	1.000
InvMM	0.997	0.899	0.994	0.842

Table 1. Detection performance on DDPM and SD v1.4. *: using training captions, fixed during inversion.

images of CelebAHQ and FFHQ are assigned infinite memorization scores. In contrast, both $\lambda = 0$ and adaptive reweighting successfully invert all images. However, Fixing λ to 0 leads to larger resulting memorization scores, which indicates underestimation of the extent of memorization.

Figure 4 illustrates the generation results with the learned distributions. With the adaptive algorithm, we are able to successfully perform inversion on various datasets and DMs. The random generated samples closely resembles the training images. The results support the premise of InvMM being a meaningful measure.

5.3. Detection

For InvMM to be a correct measure of memorization, it should be capable of distinguishing highly memorized images from normal ones. To construct a reliable test set,

we conduct a nearest neighbor test following previous studies [9, 50, 58] to discover highly memorized images from DM’s training set. In this sense, highly memorized images consist of training images that can appear at sampling time. Specifically, we consider DDPM trained on CIFAR-10, LDMs trained on CelebAHQ and FFHQ, and SD trained on LAION. With their official implementations, only DDPM and Stable Diffusion v1.4 present obvious replications, which are thus used for evaluation. Finally, for DDPM, the 99 discovered training images appearing in 1M random samples are used as positive samples and another 1k different training images are included as negative samples; for SD v1.4, we deem images in the *confirmed* set as positive and those in the *normal* set as negative.

Table 1 presents the detection performance assessed via AUC and TPR@1%FPR. For the unconditional DDPM on CIFAR-10, training loss metrics (the first 2 rows) show decent results and the original ϵ_0 -loss works much better than the x_0 -loss. The differential metric M^{LOO} is less effective than the training loss and InvMM. The results indicate that training loss based metrics (including M^{LOO}) are not reliable to signify memorization, as they are not fundamentally commensurable between samples. InvMM measures memorization of each sample by contrasting their sensitive noise distribution to a common standard Gaussian, thus having the same scale.

For SD v1.4, we compare to training loss metrics and the metric proposed by Wen et al. [61]. As the compared methods all require access to image captions, we implement the counterpart for InvMM as well. With access to captions, all the metrics achieve perfect detection performance. However, this does not mean that the compared methods can also be utilized as memorization measures. On the one hand, training captions might not be available in practice, e.g., for non-training images. On the other hand, exploiting training captions for detection is actually to predict whether the captions will replicate the training images, rather than measure the memorization. In contrast, that our measure calculated with prompt optimized simultaneously shows a degree of performance drop, implies that images considered as less memorized according to the behavior of their training captions might be actually memorized more, exposed by potential prompts. In this sense, our measure provides a worst-case estimate of memorization for conditional DMs.

5.4. Influence factors

Both theoretical analysis and empirical investigation point out that dataset complexity [15, 51], dataset size [15, 51], cardinality of latent vector set [53] and data duplication [59] are important factors for memorization. We therefore verify the correctness of our measure by utilizing it to describe tendency of memorization in the change of these factors.

Dataset complexity, size and training epoch. First of

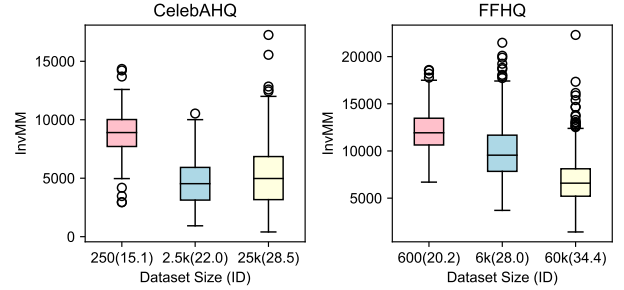


Figure 5. Dataset complexity & size vs. memorization. All the models are trained for 943 epochs on CelebAHQ and 446 epochs on FFHQ.

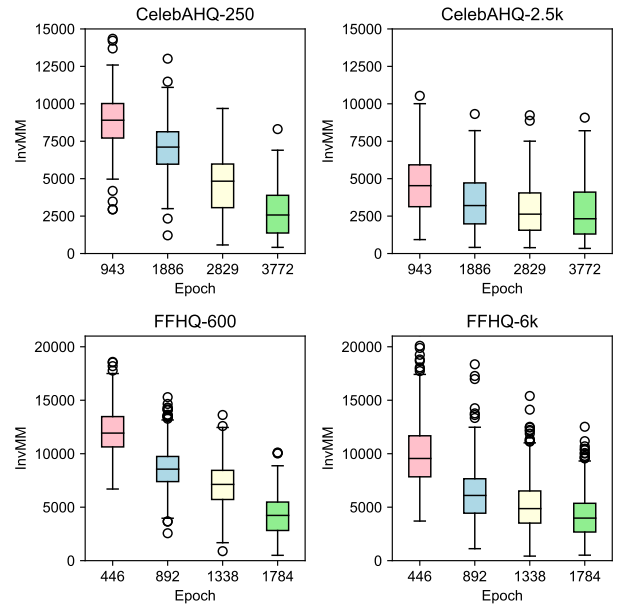


Figure 6. Training epoch vs. memorization. Models are trained for multiples of the default epoch (CelebAHQ: 943, FFHQ: 446).

all, we simultaneously validate dataset complexity, size and cardinality of latent vector set on CelebAHQ and FFHQ. Following Feng et al. [15], we measure dataset complexity with Intrinsic Dimensionality (ID) [31]. The cardinality of latent vector set can be controlled by training epochs (if in each iteration a fresh random latent vector is picked). However, we argue that previous works [15, 51] obfuscate the effect of dataset size and training epochs, as models are trained for different epochs (probably more) on smaller subsets to the full dataset. Consequently, on smaller subsets, each training image would see different number of latent vectors. Therefore, in our experiment, we decouple these two factors by training for the same epochs as on the full dataset when studying the influence of dataset size.

As can be observed in Fig. 5, dataset complexity and size

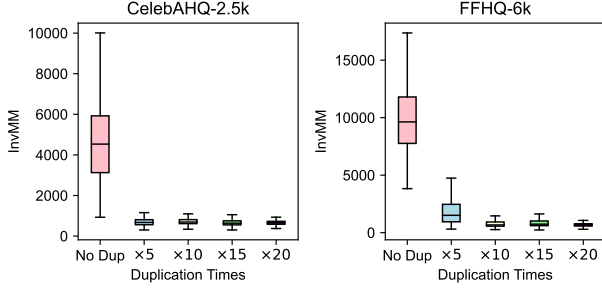


Figure 7. Duplication vs. memorization on CelebAHQ-2.5k and FFHQ-6k. CelebAHQ-250 and FFHQ-600 subsets are duplicated 5, 10, 15 and 20 times respectively. Outliers are hidden for clarity.

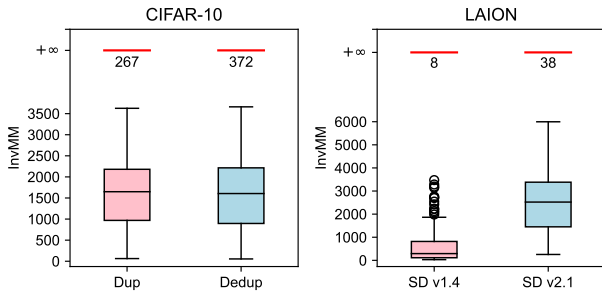


Figure 8. Deduplication vs. memorization.

seem not present high correlation with memorization, as indicated by our measure. However, when trained for longer time, the memorization scores gradually decrease, which indicates a large extent of memorization. Therefore, dataset complexity and size are not independent determining factors, and in conclusion, our measure accurately reflects the impact of these three factors on memorization.

Data duplication. We then validate the effect of data duplication in DMs’ training set through our measure. We train a series of LDMs on CelebAHQ-2.5k and FFHQ-6k, with their subsets CelebAHQ-250 and FFHQ-600 duplicated 5, 10, 15 and 20 times. Figure 7 depicts the memorization scores of duplicated images. As can be observed, data duplication largely worsens memorization in DMs and our measure is sensitive to these changes. With increasing duplication times, the larger FFHQ-6k dataset presents a stronger resistance to memorization.

For CIFAR-10 and LAION which originally contains duplicates, we observe the effect of deduplication. We deduplicate CIFAR-10 with SSCD embeddings and DBSCAN clustering [14]. This results in 666 identified clusters, only one image of which is retained for training. The memorization is evaluated on the retained 666 images before and after deduplication. On LAION, as compared to SD v1.4, SD v2.1 deduplicates the training set. The memorization

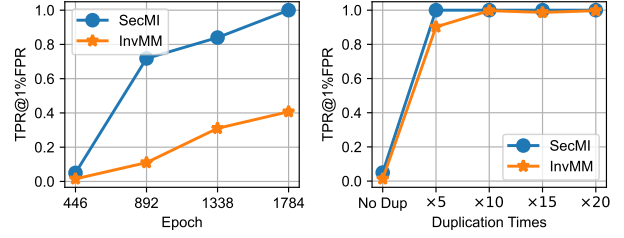


Figure 9. Performance comparison of membership inference on FFHQ-6k, across different training epochs and duplication times.

is evaluated on the *confirmed* and *suspicious* sets. Figure 8 shows the results, with infinite scores highlighted. As can be observed, InvMM clearly exhibits the benefits that deduplication brings.

5.5. Comparison to membership

A close topic to memorization is membership inference [8, 13, 48], which aims to predict whether a sample is used for training. The common accepted assumption is that member samples are fit “better” than hold-out samples [13], thus statistics like (variant of) training loss or differential training loss [8] are generally used for membership inference. A comparison to a recent membership inference metric SecMI [13] on FFHQ-6k, as shown in Fig. 9, does present a positive correlation between membership and memorization. As factors that exacerbate memorization changes, both SecMI and InvMM shows better performance.

However, there is still a performance gap between membership score and memorization score, which indicates that certain samples from the hold-out set are memorized more than some member samples. This mainly results from the gap between model’s metric (training loss) and human’s metric (perceptual similarity). Membership inference leverages the model’s metric for prediction, while memorization should resort to perceptual metric, e.g., simulated by SSCD. What level of loss leads to image replication depends both on the model and image itself. Low training loss does not necessarily lead to data replication, but would probably distinguish trained data from never accessed. On the contrary, high training loss indicating non-membership may still be enough for replication. In summary, membership does not deterministically lead to high memorization and vice versa. Our measure differs from membership inference metric by focusing on the perceptual level and adaptively handles the specific loss landscape of different samples.

6. Conclusion

In this work, we dive into measuring memorization for diffusion models. Comprehensive experiments demonstrate the ability of the proposed measure to correctly describe the

extent to which any image is memorized. In short, an image to a higher extent of memorization is able to be inverted to a more standard and diverse latent distribution. However, our method is also limited by its simple modeling of the sensitive latent noise as multivariate normal. During our research, we observed many clues confirming that the true distribution is complex. Future work might consider more advanced methods, e.g., a generative network, to fit the sensitive noise. Our measure may also support more practical applications, such as online sensitive noise filtering and adversarial training to mitigate harmful memorization.

References

- [1] Midjourney. <https://www.midjourney.com>. 1
- [2] Artist finds private medical record photos in popular AI training data set. <https://arstechnica.com/information-technology/2022/09/artist-finds-private-medical-record-photos-in-popular-ai-training-data-set/>. 1
- [3] DALL-E 3. <https://openai.com/dall-e-3>. 1
- [4] Martin Arjovsky, Soumith Chintala, and Léon Bottou. Wasserstein generative adversarial networks. In *International conference on machine learning*, pages 214–223. PMLR, 2017. 2
- [5] Sanjeev Arora and Yi Zhang. Do gans actually learn the distribution? an empirical study. *arXiv preprint arXiv:1706.08224*, 2017. 2
- [6] Tim Brooks, Bill Peebles, Connor Holmes, Will DePue, Yufei Guo, Li Jing, David Schnurr, Joe Taylor, Troy Luhman, Eric Luhman, Clarence Ng, Ricky Wang, and Aditya Ramesh. Video generation models as world simulators. 2024. 1
- [7] Tom Brown, Benjamin Mann, Nick Ryder, Melanie Subbiah, Jared D Kaplan, Prafulla Dhariwal, Arvind Neelakantan, Pranav Shyam, Girish Sastry, Amanda Askell, Sandhini Agarwal, Ariel Herbert-Voss, Gretchen Krueger, Tom Henighan, Rewon Child, Aditya Ramesh, Daniel Ziegler, Jeffrey Wu, Clemens Winter, Chris Hesse, Mark Chen, Eric Sigler, Mateusz Litwin, Scott Gray, Benjamin Chess, Jack Clark, Christopher Berner, Sam McCandlish, Alec Radford, Ilya Sutskever, and Dario Amodei. Language models are few-shot learners. In *Advances in Neural Information Processing Systems*, pages 1877–1901. Curran Associates, Inc., 2020. 2
- [8] Nicholas Carlini, Steve Chien, Milad Nasr, Shuang Song, Andreas Terzis, and Florian Tramer. Membership inference attacks from first principles. In *2022 IEEE Symposium on Security and Privacy (SP)*, pages 1897–1914. IEEE, 2022. 8
- [9] Nicolas Carlini, Jamie Hayes, Milad Nasr, Matthew Jagielski, Vikash Sehwal, Florian Tramer, Borja Balle, Daphne Ippolito, and Eric Wallace. Extracting training data from diffusion models. In *32nd USENIX Security Symposium (USENIX Security 23)*, pages 5253–5270, 2023. 1, 2, 4, 7
- [10] Nicholas Carlini, Daphne Ippolito, Matthew Jagielski, Katherine Lee, Florian Tramer, and Chiyuan Zhang. Quantifying memorization across neural language models. In *The Eleventh International Conference on Learning Representations*, 2023. 2
- [11] George Cazenavette, Avneesh Sud, Thomas Leung, and Ben Usman. Fakeinversion: Learning to detect images from unseen text-to-image models by inverting stable diffusion. In *Proceedings of the IEEE/CVF Conference on Computer Vision and Pattern Recognition*, pages 10759–10769, 2024. 3
- [12] Chen Chen, Daochang Liu, and Chang Xu. Towards memorization-free diffusion models. In *Proceedings of the IEEE/CVF Conference on Computer Vision and Pattern Recognition*, pages 8425–8434, 2024. 2
- [13] Jinhao Duan, Fei Kong, Shiqi Wang, Xiaoshuang Shi, and Kaidi Xu. Are diffusion models vulnerable to membership inference attacks? In *International Conference on Machine Learning*, pages 8717–8730. PMLR, 2023. 8
- [14] Martin Ester, Hans-Peter Kriegel, Jörg Sander, Xiaowei Xu, et al. A density-based algorithm for discovering clusters in large spatial databases with noise. In *kdd*, pages 226–231, 1996. 8
- [15] Qianli Feng, Chenqi Guo, Fabian Benitez-Quiroz, and Aleix M Martinez. When do gans replicate? on the choice of dataset size. In *Proceedings of the IEEE/CVF International Conference on Computer Vision*, pages 6701–6710, 2021. 2, 7
- [16] Rinon Gal, Yuval Alaluf, Yuval Atzmon, Or Patashnik, Amit Haim Bermano, Gal Chechik, and Daniel Cohen-or. An image is worth one word: Personalizing text-to-image generation using textual inversion. In *The Eleventh International Conference on Learning Representations*, 2023. 3
- [17] Ian Goodfellow, Jean Pouget-Abadie, Mehdi Mirza, Bing Xu, David Warde-Farley, Sherjil Ozair, Aaron Courville, and Yoshua Bengio. Generative adversarial nets. *Advances in neural information processing systems*, 27, 2014. 2
- [18] Andres Guadamuz. Photographer sues LAION for copyright infringement. <https://www.technollama.co.uk/photographer-sues-laion-for-copyright-infringement>, 2023. 1
- [19] Ishaan Gulrajani, Colin Raffel, and Luke Metz. Towards gan benchmarks which require generalization. In *International Conference on Learning Representations*, 2019. 2
- [20] Chuan Guo, Alexandre Sablayrolles, Hervé Jégou, and Douwe Kiela. Gradient-based adversarial attacks against text transformers. *arXiv preprint arXiv:2104.13733*, 2021. 5, 4
- [21] Jonathan Ho and Tim Salimans. Classifier-free diffusion guidance. *arXiv preprint arXiv:2207.12598*, 2022. 3
- [22] Jonathan Ho, Ajay Jain, and Pieter Abbeel. Denoising diffusion probabilistic models. *Advances in neural information processing systems*, 33:6840–6851, 2020. 1, 2, 3, 6
- [23] Eric Jang, Shixiang Gu, and Ben Poole. Categorical reparameterization with gumbel-softmax. *arXiv preprint arXiv:1611.01144*, 2016. 5
- [24] James Jordon, Jinsung Yoon, and Mihaela Van Der Schaar. Pate-gan: Generating synthetic data with differential privacy guarantees. In *International Conference on Learning Representations*, 2018. 2
- [25] Tero Karras, Timo Aila, Samuli Laine, and Jaakko Lehtinen. Progressive growing of GANs for improved quality, stabil-

- ity, and variation. In *International Conference on Learning Representations*, 2018. 6
- [26] Tero Karras, Samuli Laine, and Timo Aila. A style-based generator architecture for generative adversarial networks. In *Proceedings of the IEEE/CVF conference on computer vision and pattern recognition*, pages 4401–4410, 2019. 6
- [27] Diederik P. Kingma and Jimmy Ba. Adam: A method for stochastic optimization. In *3rd International Conference on Learning Representations, ICLR 2015, San Diego, CA, USA, May 7-9, 2015, Conference Track Proceedings*, 2015. 2
- [28] Diederik P. Kingma and Max Welling. Auto-encoding variational bayes. In *2nd International Conference on Learning Representations, ICLR 2014, Banff, AB, Canada, April 14-16, 2014, Conference Track Proceedings*, 2014. 3
- [29] Diederik P. Kingma and Max Welling. Auto-encoding variational bayes. In *2nd International Conference on Learning Representations, ICLR 2014, Banff, AB, Canada, April 14-16, 2014, Conference Track Proceedings*, 2014. 2
- [30] Alex Krizhevsky, Geoffrey Hinton, et al. Learning multiple layers of features from tiny images. 2009. 6
- [31] Elizaveta Levina and Peter Bickel. Maximum likelihood estimation of intrinsic dimension. *Advances in neural information processing systems*, 17, 2004. 7
- [32] Luping Liu, Yi Ren, Zhijie Lin, and Zhou Zhao. Pseudo numerical methods for diffusion models on manifolds. In *International Conference on Learning Representations*, 2022. 3
- [33] Calvin Luo. Understanding diffusion models: A unified perspective. *arXiv preprint arXiv:2208.11970*, 2022. 3
- [34] Shitong Luo and Wei Hu. Diffusion probabilistic models for 3d point cloud generation. In *Proceedings of the IEEE/CVF conference on computer vision and pattern recognition*, pages 2837–2845, 2021. 1
- [35] Ron Mokady, Amir Hertz, Kfir Aberman, Yael Pritch, and Daniel Cohen-Or. Null-text inversion for editing real images using guided diffusion models. In *Proceedings of the IEEE/CVF Conference on Computer Vision and Pattern Recognition*, pages 6038–6047, 2023. 3
- [36] Helen Nissenbaum. Privacy as contextual integrity. *Wash. L. Rev.*, 79:119, 2004. 1
- [37] Kai Packhäuser, Lukas Folle, Florian Thamm, and Andreas Maier. Generation of anonymous chest radiographs using latent diffusion models for training thoracic abnormality classification systems. In *2023 IEEE 20th International Symposium on Biomedical Imaging (ISBI)*, pages 1–5. IEEE, 2023. 2
- [38] Ed Pizzi, Sreya Dutta Roy, Sugosh Nagavara Ravindra, Priya Goyal, and Matthijs Douze. A self-supervised descriptor for image copy detection. In *Proceedings of the IEEE/CVF Conference on Computer Vision and Pattern Recognition*, pages 14532–14542, 2022. 4
- [39] Alec Radford, Jong Wook Kim, Chris Hallacy, Aditya Ramesh, Gabriel Goh, Sandhini Agarwal, Girish Sastry, Amanda Askell, Pamela Mishkin, Jack Clark, et al. Learning transferable visual models from natural language supervision. In *International conference on machine learning*, pages 8748–8763. PMLR, 2021. 3
- [40] Aditya Ramesh, Prfulla Dhariwal, Alex Nichol, Casey Chu, and Mark Chen. Hierarchical text-conditional image generation with CLIP latents. *arXiv preprint arXiv:2204.06125*, 1(2):3, 2022. 1
- [41] Robin Rombach, Andreas Blattmann, Dominik Lorenz, Patrick Esser, and Björn Ommer. High-resolution image synthesis with latent diffusion models. In *Proceedings of the IEEE/CVF conference on computer vision and pattern recognition*, pages 10684–10695, 2022. 1, 6
- [42] Chitwan Saharia, William Chan, Saurabh Saxena, Lala Li, Jay Whang, Emily L Denton, Kamyar Ghasemipour, Raphael Gontijo Lopes, Burcu Karagol Ayan, Tim Salimans, et al. Photorealistic text-to-image diffusion models with deep language understanding. *Advances in neural information processing systems*, 35:36479–36494, 2022. 1
- [43] Tim Salimans, Ian Goodfellow, Wojciech Zaremba, Vicki Cheung, Alec Radford, and Xi Chen. Improved techniques for training gans. *Advances in neural information processing systems*, 29, 2016. 2
- [44] Pamela Samuelson. Generative ai meets copyright. *Science*, 381(6654):158–161, 2023. 1
- [45] Christoph Schuhmann, Romain Beaumont, Richard Vencu, Cade Gordon, Ross Wightman, Mehdi Cherti, Theo Coombes, Aarush Katta, Clayton Mullis, Mitchell Wortsman, et al. Laion-5b: An open large-scale dataset for training next generation image-text models. *Advances in Neural Information Processing Systems*, 35:25278–25294, 2022. 1, 6
- [46] Shawn Shan, Jenna Cryan, Emily Wenger, Haitao Zheng, Rana Hanocka, and Ben Y Zhao. Glaze: Protecting artists from style mimicry by {Text-to-Image} models. In *32nd USENIX Security Symposium (USENIX Security 23)*, pages 2187–2204, 2023. 1
- [47] Taylor Shin, Yasaman Razeghi, Robert L Logan IV, Eric Wallace, and Sameer Singh. Autoprompt: Eliciting knowledge from language models with automatically generated prompts. In *Proceedings of the 2020 Conference on Empirical Methods in Natural Language Processing (EMNLP)*. Association for Computational Linguistics, 2020. 4
- [48] Reza Shokri, Marco Stronati, Congzheng Song, and Vitaly Shmatikov. Membership inference attacks against machine learning models. In *2017 IEEE symposium on security and privacy (SP)*, pages 3–18. IEEE, 2017. 8
- [49] Jascha Sohl-Dickstein, Eric Weiss, Niru Maheswaranathan, and Surya Ganguli. Deep unsupervised learning using nonequilibrium thermodynamics. In *International conference on machine learning*, pages 2256–2265. PMLR, 2015. 1, 2, 3
- [50] Gowthami Somepalli, Vasu Singla, Micah Goldblum, Jonas Geiping, and Tom Goldstein. Diffusion art or digital forgery? investigating data replication in diffusion models. In *Proceedings of the IEEE/CVF Conference on Computer Vision and Pattern Recognition*, pages 6048–6058, 2023. 2, 4, 7
- [51] Gowthami Somepalli, Vasu Singla, Micah Goldblum, Jonas Geiping, and Tom Goldstein. Understanding and mitigating copying in diffusion models. *Advances in Neural Information Processing Systems*, 36:47783–47803, 2023. 2, 7

- [52] Jiaming Song, Chenlin Meng, and Stefano Ermon. Denoising diffusion implicit models. In *International Conference on Learning Representations*, 2021. [3](#), [2](#)
- [53] N Vaishnavh, C Raffel, and IJ Goodfellow. Theoretical insights into memorization in gans. In *Neural Information Processing Systems Workshop*, 2018. [2](#), [7](#)
- [54] Gerrit van den Burg and Chris Williams. On memorization in probabilistic deep generative models. *Advances in Neural Information Processing Systems*, 34:27916–27928, 2021. [2](#), [6](#), [1](#)
- [55] Nikhil Vyas, Sham M Kakade, and Boaz Barak. On provable copyright protection for generative models. In *International Conference on Machine Learning*, pages 35277–35299. PMLR, 2023. [2](#)
- [56] Zhendong Wang, Jianmin Bao, Wengang Zhou, Weilun Wang, Hezhen Hu, Hong Chen, and Houqiang Li. DIRE for diffusion-generated image detection. In *Proceedings of the IEEE/CVF International Conference on Computer Vision*, pages 22445–22455, 2023. [3](#)
- [57] Ryan Webster. A reproducible extraction of training images from diffusion models. *CoRR*, abs/2305.08694, 2023. [2](#), [6](#)
- [58] Ryan Webster, Julien Rabin, Loic Simon, and Frédéric Jurie. Detecting overfitting of deep generative networks via latent recovery. In *Proceedings of the IEEE/CVF Conference on Computer Vision and Pattern Recognition*, pages 11273–11282, 2019. [2](#), [7](#)
- [59] Ryan Webster, Julien Rabin, Loic Simon, and Frederic Jurie. On the de-duplication of LAION-2B. *arXiv preprint arXiv:2303.12733*, 2023. [2](#), [6](#), [7](#)
- [60] Yuxin Wen, Neel Jain, John Kirchenbauer, Micah Goldblum, Jonas Geiping, and Tom Goldstein. Hard prompts made easy: Gradient-based discrete optimization for prompt tuning and discovery. In *Advances in Neural Information Processing Systems*, 2024. [4](#)
- [61] Yuxin Wen, Yuchen Liu, Chen Chen, and Lingjuan Lyu. Detecting, explaining, and mitigating memorization in diffusion models. In *The Twelfth International Conference on Learning Representations*, 2024. [2](#), [6](#), [7](#)
- [62] Xiaoyu Wu, Yang Hua, Chumeng Liang, Jiaru Zhang, Hao Wang, Tao Song, and Haibing Guan. Cgi-dm: Digital copyright authentication for diffusion models via contrasting gradient inversion. In *2024 IEEE/CVF Conference on Computer Vision and Pattern Recognition (CVPR)*, pages 10812–10821. IEEE Computer Society, 2024. [3](#)
- [63] Yuxin Zhang, Nisha Huang, Fan Tang, Haibin Huang, Chongyang Ma, Weiming Dong, and Changsheng Xu. Inversion-based style transfer with diffusion models. In *Proceedings of the IEEE/CVF conference on computer vision and pattern recognition*, pages 10146–10156, 2023. [3](#)

An Inversion-based Measure of Memorization for Diffusion Models

Supplementary Material

7. Additional technical description

7.1. A unified understanding

Similar to Eq. (2), the variational lower bound can be further lower bounded w.r.t. a conditional distribution $q_\phi(c, x_0)$ with parameters ϕ . For text-to-image models, it is instantiated as a prompt distribution $q_\phi(\omega|x_0)$.

Following similar expansion in Eqs. (3) and (4), we obtain the full inversion variational lower bound w.r.t. both condition and latent noise:

$$\log p_\theta(x_0) \geq -l_{de}(x_0; \phi, \varphi) - l_{kl}(x_0; \varphi) - l_{cr}(x_0; \phi) \quad (13)$$

and

$$\begin{aligned} l_{de}(x_0; \phi, \varphi) &= -\mathbb{E}_{q_\phi(c|x_0), q_\varphi(\epsilon_0|x_0)} [\log p_\theta(x_0|x_1, c) \\ &\quad + \sum_{t=2}^T D_{\text{KL}}(q_\varphi(x_{t-1}|x_t, x_0) \| p_\theta(x_{t-1}|x_t, c))] \end{aligned} \quad (14)$$

$$l_{kl}(x_0; \varphi) = D_{\text{KL}}(q_\varphi(x_T|x_0) \| p(x_T)) \quad (15)$$

$$l_{cr}(x_0; \phi) = D_{\text{KL}}(q_\phi(c|x_0) \| p(c)) \quad (16)$$

where l_{de} indicates the denoising error, l_{kl} is a **KL** divergence and l_{cr} is a **condition regularization** term. The three terms can be explained as the following:

1. l_{de} indicates how accurate the pretrained model denoises each x_t when the added noise is drawn from $q_\varphi(\epsilon_0|x_0)$. If l_{de} is low enough, then for most noises $\epsilon_0 \sim q_\varphi(\epsilon_0|x_0)$ the model presents low denoising error, we can anticipate that the sampling trace starting at $\epsilon_0 \sim q_\varphi(\epsilon_0|x_0)$ will head towards x_0 and finally generate x_0 .
2. l_{kl} is a normality regularizer. When l_{de} is optimized to a low level, the noise distribution $q_\varphi(\epsilon_0|x_0)$ identifies a sensitive set of noises that will cause the generation of the training image x_0 . $p(x_T)$ is the prior distribution, usually set to the standard Gaussian. In a sense, l_{kl} measures the diversity of the model's generation: When l_{kl} becomes zero, i.e., $q_\varphi(\epsilon_0|x_0)$ is standard Gaussian, then low enough l_{de} means the model always generates x_0 and loses generalization.
3. l_{cr} encourages the realistic feasibility of the condition distribution $q_\phi(c|x_0)$. For example, if $p(c)$ is considered the distribution of natural language, then minimizing l_{cr} indicates that prompt $c \sim q_\phi(c|x_0)$ should be grammatically and semantically correct.

In the standard training of diffusion model (DM), l_{kl} is ignored because $q_\varphi(\epsilon_0|x_0)$ is set to the standard Gaussian $\mathcal{N}(\mathbf{0}, \mathbf{I})$ such that $q_\varphi(x_T|x_0)$ approximately equals

$\mathcal{N}(\mathbf{0}, \mathbf{I})$, l_{kl} approximately equals zero. $q_\phi(c|x_0)$ reduces to several captions coupled with the training image such that l_{cr} is also zero.

Our idea is to measure memorization by relaxation of the noise and prompt distribution so that the denoising error can be optimized low enough to replicate the target image. Based on this, the normality of the worst-case distribution of sensitive latent noise is used as a measure.

7.2. Reparameterization

Sampling from the noise and condition distribution in Eq. (14) is non-differentiable, we indirectly sample them.

When the noise distribution is $q_\varphi(\epsilon_0|x_0)$ a multivariate Gaussian $\mathcal{N}(\mu, \sigma^2)$ with learnable mean μ and diagonal variance σ^2 ,

$$\epsilon_0 = \epsilon' \sigma + \mu, \epsilon' \sim \mathcal{N}(\mathbf{0}, \mathbf{I}) \quad (17)$$

For text-to-image DM, each token ω_i (see Sec. 4.4) is reparameterized by

$$\tilde{\omega}_{i,j} = \frac{\exp((\log \pi_{i,j} + \mathbf{g}_{i,j})/\tau)}{\sum_{k=1}^{|\mathcal{V}|} \exp((\log \pi_{i,k} + \mathbf{g}_{i,k})/\tau)} \quad (18)$$

where $\{\mathbf{g}_{i,j}\}, i = 1 \dots N, j = 1 \dots |\mathcal{V}|$ are i.i.d samples drawn from Gumbel(0, 1), τ is a temperature factor. When τ approaches 0, the smoothed sample $\tilde{\omega}_i$ becomes one-hot.

After optimization, we can draw discrete prompt from the learned $q_\phi(\omega|x_0)$ by:

$$\omega_i = \arg \max_j [\log \pi_{i,j} + \mathbf{g}_{i,j}] \quad (19)$$

8. Additional experiment details and results

8.1. Experiment setting

If not stated otherwise, the hyperparameters follow the default setting listed in Tab. 2. For CelebAHQ and FFHQ, all memorization scores in the plots are evaluated on CelebAHQ-250 and FFHQ-600. All the experiments in this paper are conducted on one NVIDIA A800 GPU.

8.2. Detection

Experiment details. On CIFAR-10, the training loss metrics are calculated on the average loss of 16 random Gaussian noise and 50 timesteps uniformly sampled within the range [1, 1000]. Following van den Burg et al. [54]'s setting, M_{LOO} is estimated using a 10-fold cross-validation. We only conduct the cross-validation once.

On LAION, the training loss metrics use 32 random Gaussian noise and 50 timesteps uniformly sampled within

	CIFAR-10	CelebAHQ	FFHQ	LAION
Learning Rate γ	1e-1	1e-1	1e-1	1e-1
Iteration S	2000	2000	2000	2000
Batch Size	32	16	16	16
Cycle C	50	10	10	50
Increment δ	1e-4	5e-4	5e-4	1e-3
Threshold ξ	1e-3	1e-3	1e-3	1e-3
Threshold β	1.0	1.0	1.0	1.0
Sampler	DDIM [52]	DDIM	DDIM	DDIM
DDIM Step	200	50	50	50
DDIM η	0	0	0	0
Optimizer	Adam [27]	Adam	Adam	Adam
SSCD Size	32×32	256×256	256×256	320×320

Table 2. Default hyperparameter settings.



Figure 10. Not invertible examples in SD v1.4. The first column shows the corresponding training images.

the range [1, 1000]. We implement Wen et al. [61] following their best performing settings.

Calibration. SSCD similarity on the low-resolution CIFAR-10 yields many false positives (non-replication with high similarity, early stopped) and false negatives (replication with low similarity, not early stopped), although it works well on the other three high-resolution datasets. We perform a manual review on the false samples and correct their early stop timesteps and scores. All the other experimental results are unchanged.

Invertibility. More than half of the images in CIFAR-10 are not invertible even if we set $\lambda = 0$ all the time. This is probably because the DDPM (34.21 M) trained on CIFAR-10 has limited capacity to memorize every training image. Images in CelebAHQ and FFHQ are all invertible. As a comparison, the LDMs trained on them have larger capacity (314.12 M). There are also some images not invertible in Stable Diffusion. However, setting $\lambda = 0$ could invert them almost perfectly. The invertibility of an image is specific to a set of hyperparameter settings. Although it is possible to invert everything in SD, we regard samples not invertible in our setting “insignificant”, as compared to those that are easy to invert. Figure 10 shows three examples that are not invertible in SD v1.4 from the *normal* subset, as judged by SSCD. It shows that it is quite subjective to judge the similarity between images. Human may regard such cases as replication as the generated images mimic the style of training image or else. From a technical perspective, we leave

this problem untouched and follow the decision of SSCD.

8.3. Collate InvMM with nearest neighbor test

We provide another quantitative metric to collate InvMM with the nearest-neighbor test: if a training image is replicated by its nearest neighbors in randomly generated samples, then its InvMM should be small among a list of training images, and vice versa. Let S_{nn} be the set of images that expose replication in randomly generated samples, and S_{InvMM} be the same-size set of images with the lowest InvMMs in a list of images. We define the consistence between InvMM and nearest-neighbor test as the Intersection over Union (IoU) between S_{InvMM} and S_{nn} :

$$IoU = \frac{|S_{InvMM} \cap S_{nn}|}{|S_{InvMM} \cup S_{nn}|}, |S_{nn}| > 0 \quad (20)$$

Under the setting in Sec. 5.3, InvMM achieves an IoU of 0.817 on CIFAR-10 and 1.0 on LAION. The results on CelebAHQ and FFHQ are summarized in Tab. 3. 10k random samples are used to obtain the results. A random sample of cosine similarity larger than 0.5 with any training sample is considered a replication. InvMM presents consistence with the results of nearest neighbor test, indicating its potential to expose risk of training image leakage, especially when a large number of training images are prone to leakage. The 10k samples is not an adequate sampling of the large latent space ($64 \times 64 \times 3$), the performance can be refined with a larger scale of evaluation.

8.4. Comparison to membership

Experiment details. Figure 9 is evaluated with LDM trained on FFHQ-6k. FFHQ-600 is used as the member set and CelebAHQ-250 is the hold-out set. The statistic variant of SecMI is implemented following their official settings, with $t_{SEC} = 100$ and $k = 10$.

Results. Figure 11 provides quantitative evidence that different samples could be replicated with different levels of training loss. The replication loss is calculated over the inverted latent noise distribution. It shows that although hold-out samples have a larger training loss over the $\mathcal{N}(0, I)$, supporting effective membership inference, it is still possible to replicate some of them by reducing their training loss to a level higher than some of the members.

We visualize the top-2 false positives and false negatives in Fig. 12. The results show that hold-out samples are also replicated near identically.

The result further highlights the difference between membership and memorization: training loss does not completely determine data replication.

9. Ablation study on prompt inversion

This section elaborates the influence of several factors for prompt inversion in SD, including the temperature τ in

Setting	CelebAHQ-250	CelebAHQ-2.5k	FFHQ-600	FFHQ-6k	CelebAHQ	FFHQ
Default	N/A(0)	N/A(0)	N/A(0)	N/A(0)	N/A(0)	N/A(0)
Epoch $\times 2$	0.059(9)	N/A(0)	N/A(0)	N/A(0)	-	-
Epoch $\times 3$	0.326(120)	N/A(0)	0.000(1)	N/A(0)	-	-
Epoch $\times 4$	0.567(181)	0.000(3)	0.000(4)	N/A(0)	-	-
Duplicate $\times 5$	-	0.182(65)	-	0.000(2)	-	-
Duplicate $\times 10$	-	0.852(237)	-	0.192(186)	-	-
Duplicate $\times 15$	-	0.937(245)	-	0.401(323)	-	-
Duplicate $\times 20$	-	0.819(231)	-	0.434(375)	-	-

Table 3. Performance of collating InvMM with nearest neighbor test. Each result refers to IoU(NumberOf replicated training images).

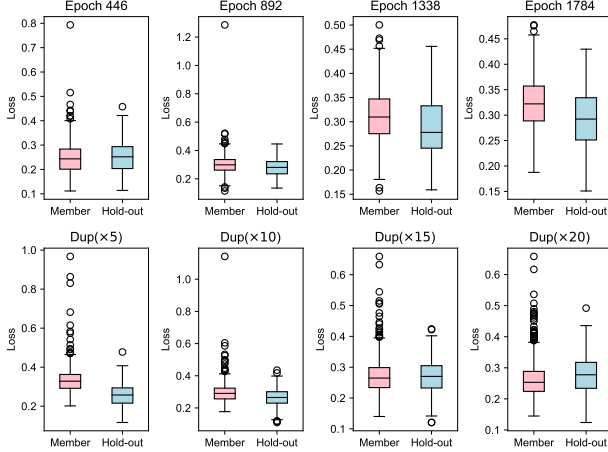


Figure 11. Comparison of replication loss for members and hold-out samples.



Figure 12. Top-2 false positives with lowest InvMM from the hold-out set and top-2 false negatives with highest InvMM from the member set. The results come from LDM trained on FFHQ-6k for 1784 epochs.

Gumbel-Softmax, the Classifier-Free Guidance (CFG) [21] scale γ and the advantage of predicting the image rather than noise for inversion (Eq. (12)). For this goal, the noise distribution is temporarily fixed to the standard Gaussian. Experiment results will show that heavily memorized images can also be uncovered in this setting.

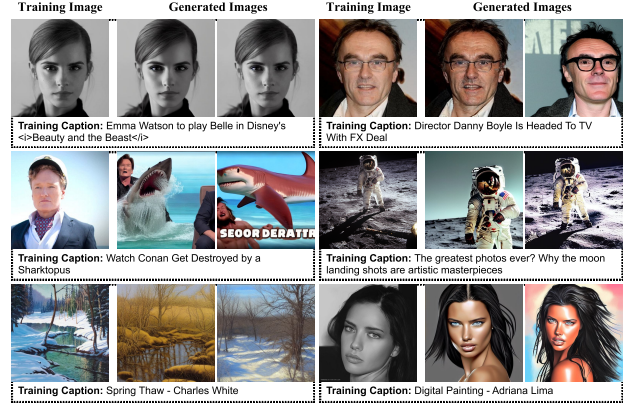


Figure 13. Examples in confirmed, suspicious and normal subsets from top to down. In each block, the right two columns show generated images using their training captions but different initial noises.

9.1. Dataset

We use the aforementioned three LAION subsets for evaluation. Figure 13 presents examples from the three subsets, together with images generated using their training captions.

9.2. Experiment setup

We utilize SD v1.4 for evaluation, which uses CLIP [39] to encode input prompts and generate high-resolution 512×512 images. The text encoders by default accepts a maximum length of 77 tokens, in which the first and last tokens are padded tokens indicating the start and end of a prompt. The rest 75 tokens are all optimized in our experiments. During optimization, the parameters θ of diffusion models are fixed. We optimize for 500 iterations with a constant learning rate of 0.2. ϕ is initialized to 0 at the beginning of optimization.

9.3. Influence of temperature

Hard prompt inversion to exactly reconstruct certain images is a challenging problem as it requires to search over a large

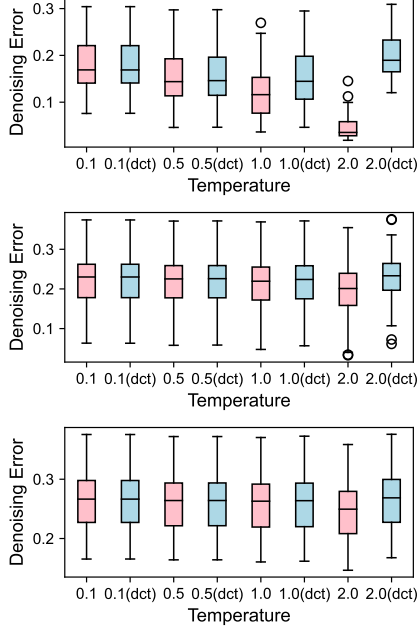


Figure 14. The distribution of denoising error of the confirmed, suspicious and normal subsets. "dct" means plus discretization.

and discrete space consisting of tens of thousands of tokens (49408 in CLIP). We have found that the convergence of inversion relies on appropriate choice of the temperature τ in Gumbel-Softmax smoothing. With τ approaching 0, $\tilde{\omega}$ drawn from the prompt distribution approaches one-hot and accurately matches a token, while it is difficult to optimize through gradient decent. Larger τ provides a smoother landscape of the target loss function and thus is easier to optimize. However, the smoothed $\tilde{\omega}$ cannot directly correspond to some tokens. Discretizing them anyway (Eq. (19)) might not preserve the same effectiveness as the smooth counterparts.

Denoising error. We first analyze the denoising error of the inverted prompt distribution when optimized with different temperatures. We consider 4 settings for the temperature to be either 0.1, 0.5, 1 or 2, as well as whether to discretize the smoothed tokens $\tilde{\omega}$ to ω . After optimization, random prompts and noises can be drawn from $q_\phi(\omega|x_0)$ and $\mathcal{N}(\mathbf{0}, \mathbf{I})$. For each image, we randomly sample 10 prompts and 10 noises for each sampled prompt, resulting in 100 prompt-noise pairs. The denoising error is estimated using 50 timesteps uniformly sampled within the range [1, 1000] and averaged over the 100 prompt-noise pairs.

The results can be seen in Fig. 14. For any type of image from different groups, higher temperatures lead to lower denoising errors on average, indicating a more adequate optimization. However, meanwhile, plus token discretization worsens the effectiveness.

Convergence. Figure 15 shows the denoising errors at each optimization step of the 6 example images in Fig. 13. For the assessment of convergence, we draw a baseline denoising error calculated using the training caption of each image. As can be observed, large temperatures induce better convergence and the difference between $\tilde{\omega}$ and ω becomes prominent. Figure 16 illustrates the generation results using prompts sampled from the learned distribution, with a CFG scale of 7. As can be seen, with $\tau = 2$, the inverted prompts are able to replicate the training images for the 4 examples from the confirmed and suspicious groups, the two from the suspicious group are newly found through our analysis. However, $\tau = 2$ plus discretization produces completely irrelevant images. Lower temperatures 0.5 and 1.0 present more consistent generation between smooth and discrete prompts, while they only produce similar images to the training ones, showing analogous content, color, etc. The smallest $\tau = 0.1$ fails to capture the main content of the training images but remains the best consistency for discretization.

Prompt distribution. Figure 17 depicts the density distribution of the entropy $-\sum_{j=1}^{|\mathcal{V}|} \pi_{i,j} \log \pi_{i,j}$ of the learned prompt categorical distributions. When $\tau = 2$, most tokens follow a high entropy distribution, which means that they are well smoothed and take an interpolation of hard tokens. In contrast, smaller temperatures produce more sharp distributions, while less effective as large temperature for inversion.

Conclusion. For the goal of effective analysis, we adopt a compromise setting with the temperature τ of 2.0 and without discretization, to reach adequate optimization. Although this violates the goal of inverting realistic prompts, it is reasonable and enough for developers to analyze the vulnerability of their models. Note that it still offers a certain level of restriction to the learned soft prompts, as the Gumbel-Softmax approximation together with a linear combination of pretrained token embeddings bound the smoothed tokens $\tilde{\omega}$ in the convex hull of the pretrained tokens.

9.4. Alternative prompt tuning methods

We also compare to several existing discrete prompt tuning methods, to see if they work for training image inversion. Figure 16 has shown that GBDA [20] fails ($\tau = 1.0$ with discretization). We further study the effectiveness of AutoPrompt [47] and PEZ [60]. AutoPrompt and PEZ are implemented following their default settings. We evaluate with 4 heavily memorized images (almost 100% sensitivity on their captions). In addition to optimizing all the 75 tokens, we also set the number of optimizable tokens the same as the corresponding training captions (shorter), to reduce the difficulty of inversion. Figure 18 shows the inversion results. AutoPrompt and PEZ both fail to reconstruct the

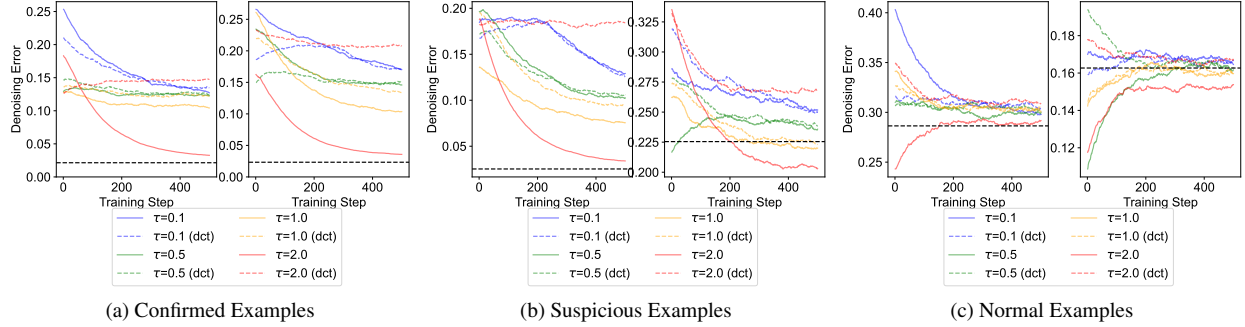


Figure 15. Training denoising error of examples from each group under different temperatures, smoothed via exponential moving average with a momentum of 0.99. "dct" means plus discretization. The black dashed line is the baseline error calculated using their training captions over 1600 randomly sampled Gaussian noises.

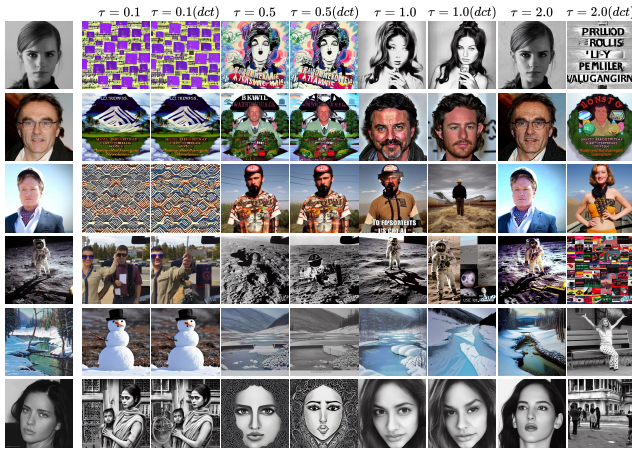


Figure 16. Generation results of different temperatures. The first column shows the corresponding training images.

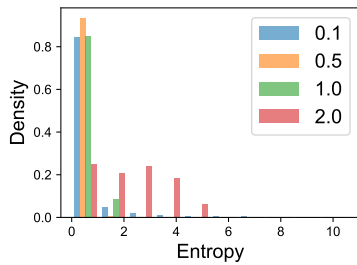


Figure 17. Entropy density distribution of the prompt categorical distribution.

original training images.

Conclusion. Existing discrete prompt tuning methods cannot effectively work to eidetically reconstruct training images. We temporarily resort to relaxed prompt tuning.



Figure 18. Inversion results of AutoPrompt and PEZ. Within each block, left: optimize 75 tokens, right: optimize tokens equal to training captions.

9.5. CFG Scale

In addition, we sweep the CFG scale γ from 0 to 7 with interval 1 to study its influence. $\gamma = 0$ indicates unconditional generation and $\gamma = 1$ indicates conditional generation without penalizing unconditional prediction. The generation results of the examples in Fig. 13 are shown in Fig. 19.

It can be observed that the generated images with $\gamma = 0$ are quite random because they only depend on the random initial noises. When $\gamma \geq 1$, for heavily memorized images in the confirmed and suspicious group, the generation results progressively converge to the training images. At times the generated images with small CFG scale only resemble the training images but are not eidetic, e.g., the 2nd to 4th rows. Nonetheless, we also discovered perfect replication for these examples with a small $\gamma = 1$ gen-

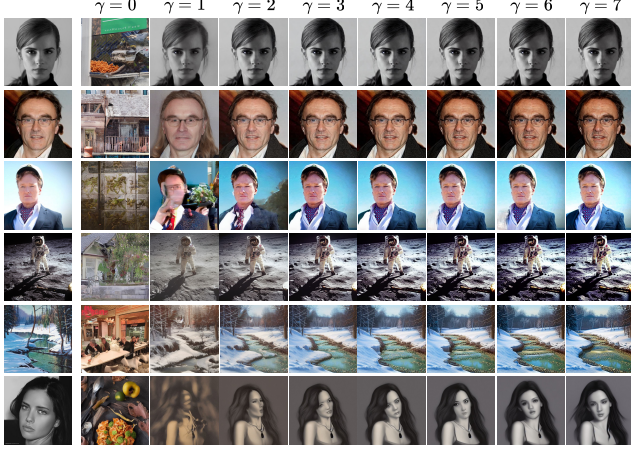


Figure 19. Generation results of different classifier-free guidance scales. The first column shows the corresponding training images.

erated using other different initial noises. This indicates that the extent to which different training images are memorized varies, and, moreover, a relatively low-level training time memorization ($\gamma = 1$) can be amplified by sampling-time options such as larger γ . Given that we optimize the prompts w.r.t. the conditional model ($\gamma = 1$), it demonstrates that training data leakage roots in the conditional model.

In addition, a gradual sharpening can be observed in the generated images as the guidance scale increases. As we optimize w.r.t. the conditional model, i.e., $\gamma = 1$, it is of enough denoising accuracy to generate an training image with relatively lower scales. Enlarging the conditional scale, however, results in excessive alignment with the input prompt. In contrast, for the images in the normal group (see the last two rows of Fig. 19), as the inverted prompt distribution cannot fully capture its complete content, generation with $\gamma = 1$ is somewhat fuzzy. It thus benefits from an increase of γ for higher quality.

Conclusion. Training data memorization can be amplified by CFG scale. As we consider the worst-case memorization in this paper, we count in the replication caused by any CFG scale from 1 to 7.

9.6. Optimization Objective

As we adopt the modified x_0 -prediction objective different from the original ϵ_0 -prediction objective of the diffusion models used in our experiments, we verify the effectiveness of x_0 -prediction over ϵ_0 -prediction for inversion. We evaluate using the images in the *confirmed* set to determine if the ϵ_0 -prediction can successfully replicate them. Figure 20 shows the inversion results of ϵ_0 -prediction. Inversion with ϵ_0 -prediction is much unstable compared to x_0 -prediction, which demonstrates the importance of reweighting denoising error at different timesteps. More specifically, the later

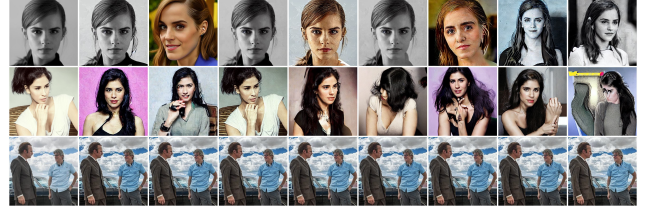


Figure 20. Inversion results of ϵ_0 -prediction. The first column shows the corresponding training images.

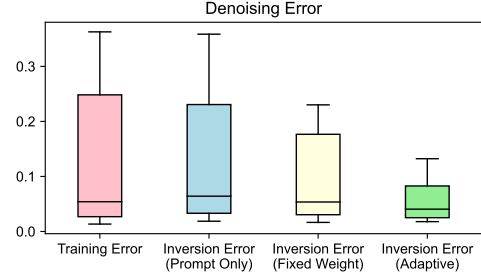


Figure 21. Comparison of inversion denoising error under different settings on SD v1.4.

timesteps at training time (earlier at sampling time) tend to shape the large scale image features [22], e.g., shape, object. Therefore, it would be beneficial to upweight the later timesteps by x_0 -prediction to more accurately guide diffusion models to generate the corresponding training images.

Conclusion. Although not aligning with the original training objective, x_0 -prediction is more stable for inversion.

9.7. Adaptive algorithm

A comparison of the (1) training error (using training captions), (2) inversion error with only prompt distribution learned, (3) inversion error with both prompt and noise distributions learned, fixing $\lambda = 1$ and (4) inversion error with both prompt and noise distributions learned, dynamically adjusting λ by Algorithm 1, is shown in Fig. 21. Compared to the training error, (2) only reduces that of heavily memorized images for which the input prompts plays a crucial role. (3) further reduces the denoising error but cannot work for all samples. Algorithm 1 can successfully reduce the denoising error of any training samples by adaptively adjusting the weight of normality regularization.

9.8. Full results

Based on the previous ablation study, we investigate memorization with the appropriate choice of each factor. In addition to SD v1.4, we include SD v2.1 for comparison. When not otherwise specified, experiment settings are the same as ablation study.

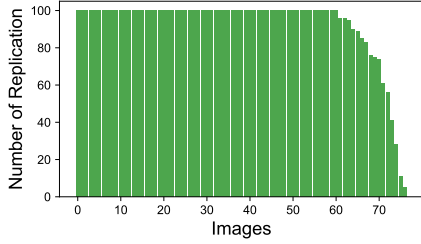


Figure 22. Number of training data replication in the confirmed group, sorted in descending order.



Figure 23. Inversion results on SD v2.1 (Fixed noise distribution). The first column shows the corresponding training images.

We first conduct a complete check of generation results. For each training image, 10 random prompts are sampled from $q_\phi(\omega|x_0)$ and for each sampled prompt, 100 Gaussian noises are sampled from $\mathcal{N}(\mathbf{0}, \mathbf{I})$. With an array of CFG scales, each prompt results in 700 randomly generated images. We manually count the number of generated images that present an obvious replication of the corresponding training image and report the maximum number of replications among the 10 prompts.

Figure 22 shows the results of the *confirmed* set for SD v1.4. There are 61 images being 100% replicated and the rest 15 images are replicated at least 5 times and at most 96 times. In the *suspicious* set, there are 3 newly discovered images that are replicated 53, 100 and 87 times. This demonstrates the advantage of our inversion-based analysis method, because some images cannot be directly generated by their training captions but do present a relatively large extent of memorization, compared to images in the *normal* set, where we found no replication.

For SD v2.1, we have not observed any replication but very similar generations, shown in Fig. 23. This is probably because SD v2.1 deduplicated the training set, and thus the true likelihood of previous duplicate samples in the training set is significantly reduced.

The counts demonstrate that training images are memorized to varied extent: For some images, training data leakage is certain to happen, for some images, it happens by chance and for the other images, it hardly happens. We also examine the images that present partial replication in our experiments by generating using their training captions and

find that indeed, they are not memorized as severely as those that are completely memorized. It thus motivates us to find a measure to tell the difference.

10. More generation results

Figures 24 to 31 show more generated images using inverted noise vectors (and prompts).



Figure 24. Random samples of SD v1.4 inversion on the *confirmed* subset. The first column shows the corresponding training images.

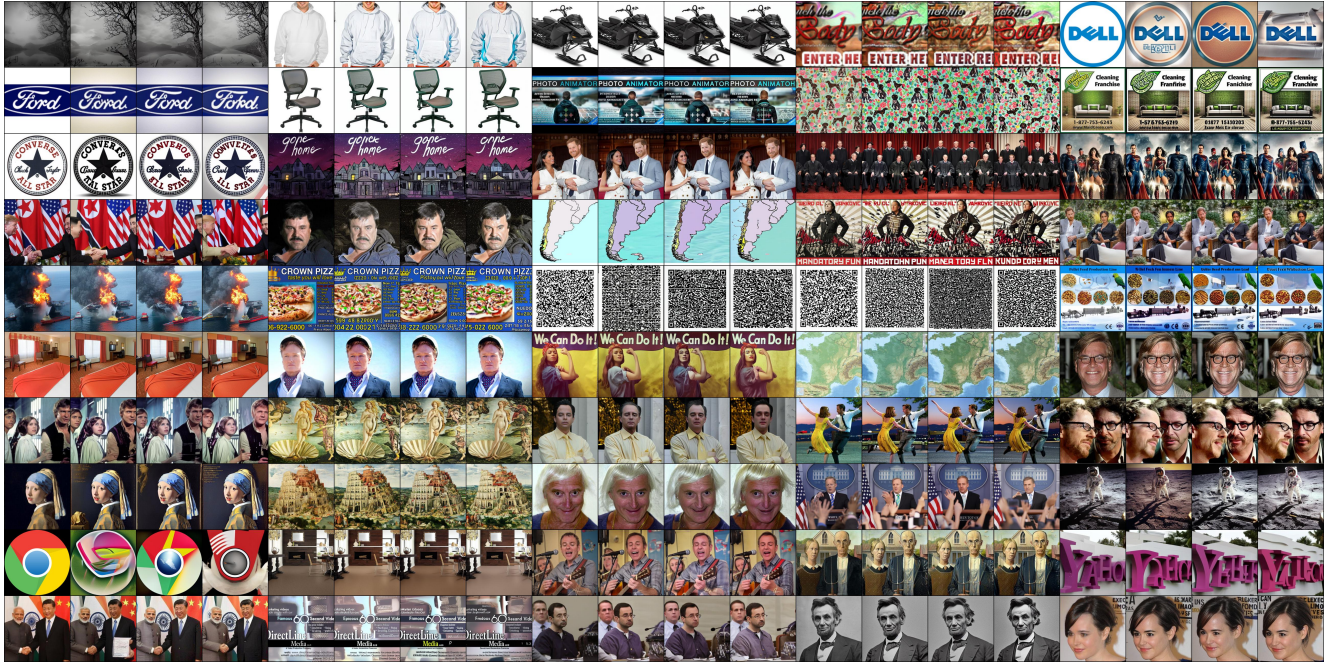


Figure 25. Random samples of SD v1.4 inversion on the *suspicious* subset. The first column shows the corresponding training images.



Figure 26. Random samples of SD v1.4 inversion on the *normal* subset. The first column shows the corresponding training images.



Figure 27. Random samples of SD v2.1 inversion on the *confirmed* subset. The first column shows the corresponding training images.

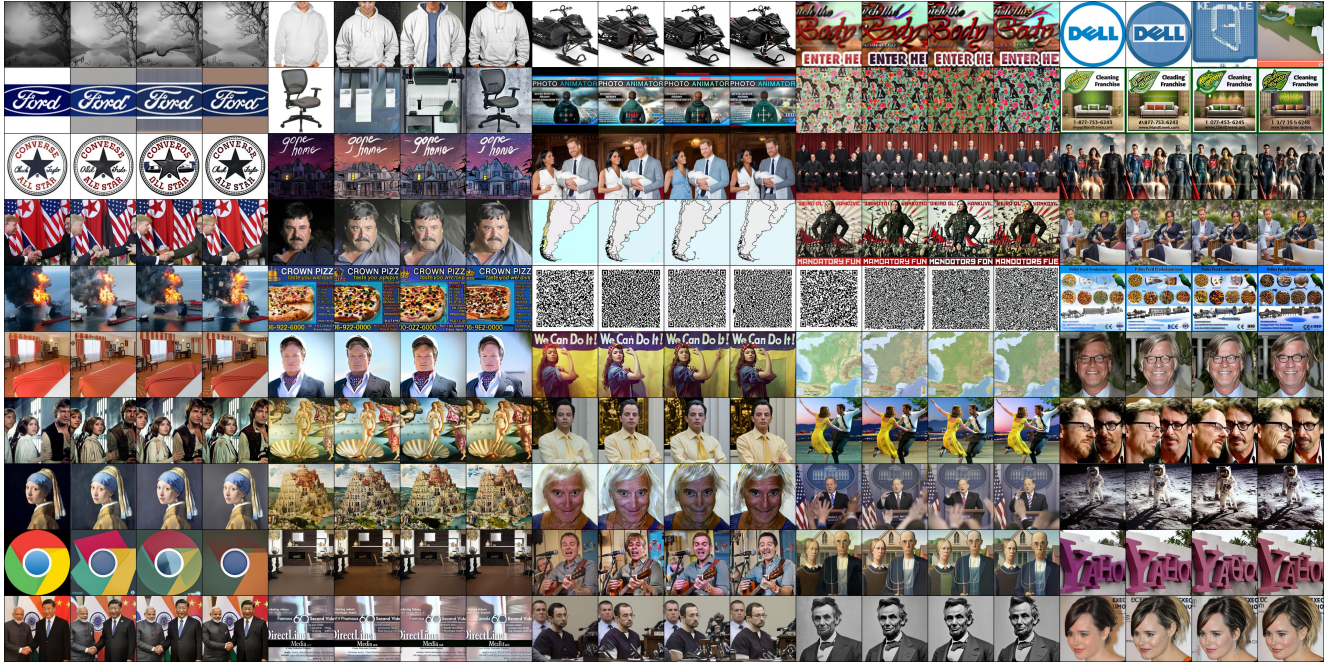


Figure 28. Random samples of SD v2.1 inversion on the *suspicious* subset. The first column shows the corresponding training images.

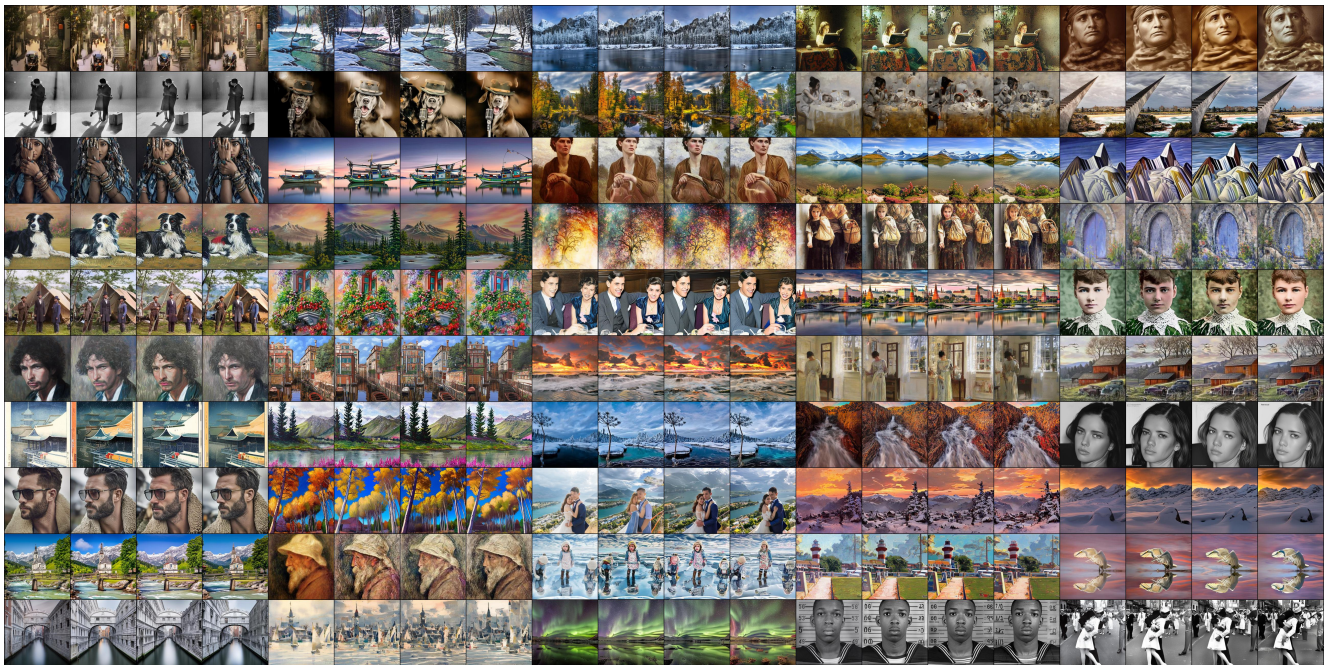


Figure 29. Random samples of SD v2.1 inversion on the *normal* subset. The first column shows the corresponding training images.



Figure 30. Random samples of LDM inversion on CelebA HQ. The first column shows the corresponding training images.



Figure 31. Random samples of LDM inversion on FFHQ. The first column shows the corresponding training images.